



Composite Fermions with Tunable Fermi Contour Anisotropy

D. Kamburov, Yang Liu, M. Shayegan, L. N. Pfeiffer, K. W. West, and K. W. Baldwin
Department of Electrical Engineering, Princeton University, Princeton, New Jersey 08544, USA
(Received 11 February 2013; published 13 May 2013)

The composite fermion formalism elegantly describes some of the most fascinating behaviors of interacting two-dimensional carriers at low temperatures and in strong perpendicular magnetic fields. In this framework, carriers minimize their energy by attaching two flux quanta and forming new quasiparticles, the so-called composite fermions. Thanks to the flux attachment, when a Landau level is half-filled, the composite fermions feel a vanishing effective magnetic field and possess a Fermi surface with a well-defined Fermi contour. Our measurements in a high-quality two-dimensional hole system confined to a GaAs quantum well demonstrate that a parallel magnetic field can significantly distort the hole-flux composite fermion Fermi contour.

DOI: [10.1103/PhysRevLett.110.206801](https://doi.org/10.1103/PhysRevLett.110.206801)

PACS numbers: 73.43.-f, 71.10.Pm, 71.18.+y, 73.21.Cd

High-quality two-dimensional (2D) carrier systems offer rich opportunities for exploring new physical phenomena. At very low temperatures and in the presence of a strong perpendicular magnetic field (B_{\perp}), the electron-electron interaction in these systems leads to a variety of remarkable many-body phases, examples of which include the fractional quantum Hall effect (FQHE) state, the Wigner crystal, and the nonuniform density phases such as stripe and bubble phases [1–3]. The FQHE can be successfully described through the concept of composite fermions (CFs), quasiparticles formed by the attachment of two (or in general an even number of) flux quanta to each carrier in high B_{\perp} [3–9]. At the applied magnetic field $B_{\perp,1/2}$ where the lowest Landau level is exactly half-filled ($\nu = 1/2$), the flux attachment completely cancels this external field, leaving the CFs as if they are at zero *effective* magnetic field. The effective field the CFs feel away from $\nu = 1/2$ is given by $B_{\perp}^* = B_{\perp} - B_{\perp,1/2}$ [10]. At and near $\nu = 1/2$, analogously to the low-field carriers, the CFs occupy a Fermi sea with a well-defined Fermi contour.

The existence of a CF Fermi contour raises the question whether any low-field Fermi contour anisotropy is transmitted to the high-field CFs after fermionization [11,12]. This issue was partially addressed in a recent experimental study of 2D electrons confined to an AlAs quantum well where they have an anisotropic (elliptical) Fermi contour [12]. The study revealed that, qualitatively similar to their $B_{\perp} = 0$ electron counterparts, CFs also exhibit a *transport* anisotropy. Namely, the resistance at $\nu = 1/2$ is larger along the long axis of the $B_{\perp} = 0$ electron Fermi contour (where the effective mass is large) compared to the resistance along the short axis (where the effective mass is smaller). While this observation suggests that the CFs might also possess an anisotropic Fermi contour, it does not provide conclusive or quantitative evidence for such anisotropy. An anisotropy in the CF scattering time, for example, would also lead to anisotropic transport. More generally, the problem of anisotropy in FQHE phenomena

has sparked recent interest both experimentally and theoretically [13–17]. Here, we report direct measurements evincing that the CF Fermi contour can be anisotropic. Moreover, we demonstrate that the anisotropy is tunable via the application of a strong magnetic field parallel to the 2D plane.

Figure 1 highlights the main ingredients of our Letter. Imagine an isotropic 2D system in which the charged particles have a circular Fermi contour (in reciprocal

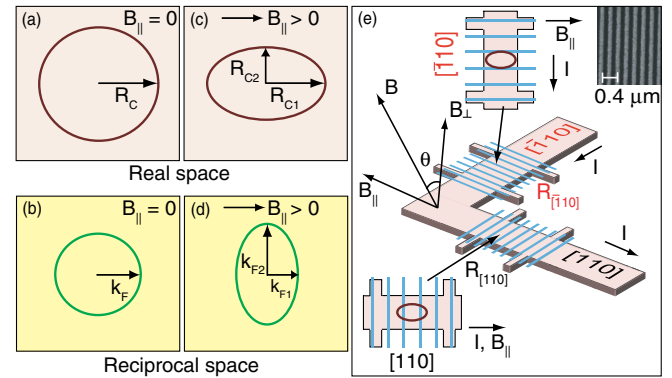


FIG. 1 (color online). (a), (b) The cyclotron orbit and the Fermi contour are shown, respectively, for an isotropic 2D system when $B_{\parallel} = 0$. (c), (d) If the 2D system has a finite (nonzero) thickness, applying $B_{\parallel} > 0$ distorts the cyclotron orbit and the Fermi contour. (e) The sample has two Hall bars along the perpendicular directions $[110]$ and $[\bar{1}10]$, and B_{\parallel} is introduced along the $[110]$ direction by tilting the sample with respect to the magnetic field direction. The electron-beam resist grating covering the top surface of each Hall bar is shown as gray (blue) stripes. The orientations of the Hall bars and the resist gratings are chosen to probe the Fermi contours in the $[110]$ and $[\bar{1}10]$ directions. The cyclotron orbits, given with brown lines, are shown for the case when the orbit diameter fits the grating period a in the $[\bar{1}10]$ direction but is larger than a in the $[110]$ direction. Inset: scanning electron microscope image of the electron-beam resist grating with an $a = 200$ nm period.

space) with Fermi wave vector k_F [Fig. 1(b)]. In a small, purely perpendicular, magnetic field the particles' classical cyclotron orbit is also circular and is completely characterized by the cyclotron radius R_C [Fig. 1(a)]. Now, if the particles have a finite (nonzero) layer thickness, a parallel magnetic field (B_{\parallel}) applied in the 2D plane couples to their out-of-plane orbital motion and leads to a deformation of the cyclotron orbit, shrinking its diameter in the in-plane direction perpendicular to B_{\parallel} [Fig. 1(c)]. Equivalently, the particles' Fermi contour becomes elongated in the direction perpendicular to B_{\parallel} [Fig. 1(d)].

The Fermi contour and/or the cyclotron orbit deformation can be directly probed in a sample with a small, periodic, one-dimensional, density modulation where the carriers complete ballistic cyclotron orbits: whenever the orbit diameter becomes commensurate with the period of the density modulation, the sample's magnetoresistance exhibits a resistance minimum. In particular, the anisotropy of the cyclotron orbit or the Fermi contour can be determined via measuring the positions of the commensurability magnetoresistance minima along the two perpendicular arms of an L -shaped Hall bar as shown in Fig. 1(e). In a recent study, using the technique described in Fig. 1, we indeed measured the Fermi contour anisotropy of 2D hole systems confined to a GaAs quantum well and found that the contour is severely distorted when the 2D holes are subjected to a strong B_{\parallel} of the order of 10 T [18]. In the work described here, we use similar samples and techniques to demonstrate that the Fermi contour of the hole-flux CFs is also distorted when a strong B_{\parallel} is applied, although the degree of anisotropy is much smaller.

We studied strain-induced superlattice samples with lattice periods of $a = 175$ and 200 nm from a 2D hole system confined to a 175 Å wide GaAs quantum well grown via molecular beam epitaxy on a (001) GaAs substrate. The quantum well, located 131 nm under the surface, is flanked on each side by 95 nm thick $\text{Al}_{0.24}\text{Ga}_{0.76}\text{As}$ spacer layers and C δ -doped layers. The 2D hole density at $T \approx 0.3$ K is $p \approx 1.5 \times 10^{11} \text{ cm}^{-2}$, and the mobility is $\mu = 1.2 \times 10^6 \text{ cm}^2/\text{Vs}$. As schematically illustrated in Fig. 1(e), the sample has two Hall bars, oriented along the [110] and $[\bar{1}10]$ directions. The Hall bars are covered with periodic gratings of negative electron-beam resist. Through the piezoelectric effect in GaAs, the resist pattern induces a periodic density modulation [18–24]. We passed current along the two Hall bar arms and measured the longitudinal resistances along the arms in tilted magnetic fields, with θ denoting the angle between the field direction and the normal to the 2D plane; see Fig. 1(e). The sample was tilted around the $[\bar{1}10]$ direction so that B_{\parallel} was always along [110]. We performed the experiments using low-frequency lock-in techniques in two ^3He refrigerators with base temperatures of $T \approx 0.3$ K, one with an 18 T superconducting magnet and the other with a 31 T resistive magnet.

The high-field data (Fig. 2), taken at $\theta = 0^\circ$ ($B_{\parallel} = 0$), for the two Hall bars of the $a = 200$ nm sample exhibit prominent commensurability features around $\nu = 1/2$: a characteristic, V-shaped, resistance dip centered at $\nu = 1/2$ and two strong resistance minima, marked by arrows on each side of $\nu = 1/2$, followed by flanks of rapidly rising resistance [24–31]. Of particular interest to us are the two minima as they correspond to the commensurability of the CF cyclotron orbit diameter ($2R_C^*$) with the period a of the potential modulation. Quantitatively, for a circular CF Fermi contour, the positions of these resistance minima are given by the magnetic commensurability condition [24–32],

$$\frac{2R_C^*}{a} = \frac{5}{4}, \quad (1)$$

where $R_C^* = \hbar k_F^*/eB_{\perp}^*$ is the CF cyclotron radius at B_{\perp}^* , $k_F^* = \sqrt{4\pi p}$ is the CF Fermi wave vector, and p is the 2D hole density [10]; note that the expression for k_F^* takes into account complete spin polarization at high fields and is larger than its low-field hole counterpart by a factor of $\sqrt{2}$. In a recent study, it was demonstrated that Eq. (1) indeed describes the positions of resistance minima exhibited by hole-flux CFs in our samples in the absence of B_{\parallel} [24]; this is seen in Fig. 2 where the arrows point to the positions of the minima expected from Eq. (1). In the present study, we monitor the shift in the observed positions of these minima as a function of applied B_{\parallel} to directly probe the size and shape of the CF Fermi contour.

As illustrated in Fig. 3, the application of B_{\parallel} has a profound effect on the appearance of the commensurability minima near $\nu = 1/2$. Data for the two Hall bars along the [110] and $[\bar{1}10]$ directions are shown side-by-side in Figs. 3(a) and 3(b). In both panels, the vertical green dashed lines mark the expected positions of the CF

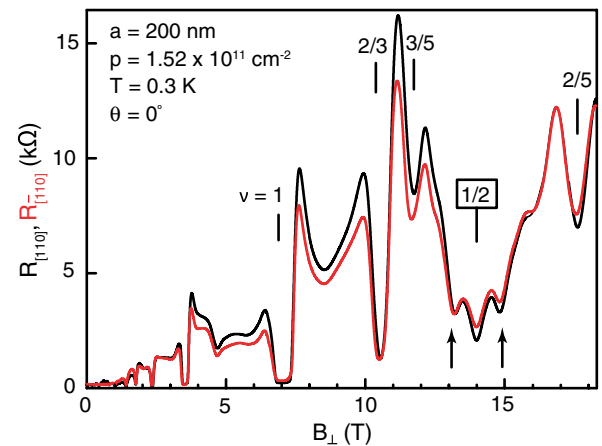


FIG. 2 (color online). Magnetoresistance traces from the [110] and $[\bar{1}10]$ Hall bars of a sample with $a = 200$ nm are shown in black and gray (red), respectively. The two prominent resistance minima visible near $\nu = 1/2$, marked by arrows, signal the commensurability of the CF cyclotron orbit diameter with the period of the density modulation (see text).

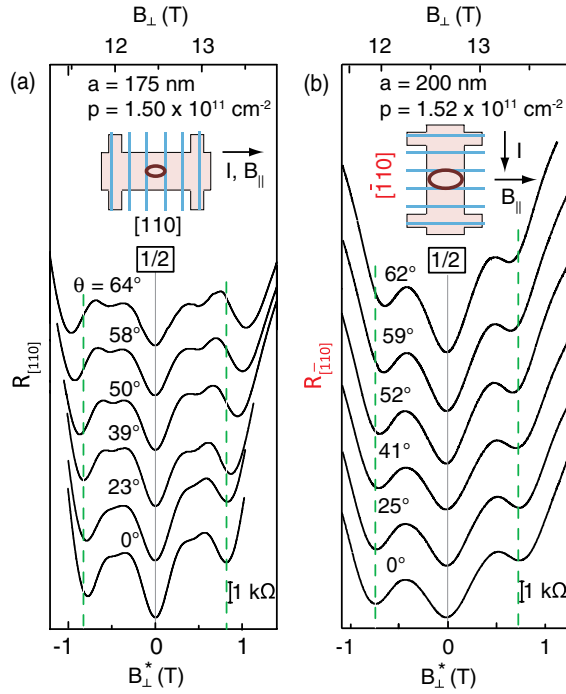


FIG. 3 (color online). (a) Summary of the evolution of the magnetoconductance in the vicinity of $\nu = 1/2$ of the $a = 175$ nm sample measured along the $[110]$ Hall bar. The tilt angle θ is given for each trace. The vertical green dashed lines mark the expected positions of the primary CF commensurability resistance minima if the CF cyclotron orbit were circular. (b) Magnetoconductance data for the $a = 200$ nm sample measured along the $[\bar{1}10]$ Hall bar. In both (a) and (b), the scale for the applied external field B_{\perp} is shown on top while the scale for the effective magnetic field $B_{\perp}^* = B_{\perp} - B_{\perp,1/2}$ felt by the CFs is given at the bottom ($B_{\perp,1/2}$ is the external field at $\nu = 1/2$).

commensurability resistance minima based on Eq. (1). These dashed lines match very well the observed positions of the resistance minima for the bottom traces of Fig. 3 which were taken at $\theta = 0$ ($B_{\parallel} = 0$) [33]. With increasing θ and B_{\parallel} , for the $[110]$ Hall bar [Fig. 3(a)], the positions of the two resistance minima shift away from the dashed lines to higher values of $|B_{\perp}^*|$. As evidenced by the top trace in Fig. 3(a), their shift reaches ≈ 0.25 T at the highest θ ($= 64^\circ$). In contrast, the positions of the resistance minima for the Hall bar in the perpendicular, $[\bar{1}10]$ direction [Fig. 3(b)] move toward lower $|B_{\perp}^*|$, and the shift is smaller. In particular, when $\theta = 62^\circ$, the minima of the top trace have moved toward $B_{\perp}^* = 0$ only by ≈ 0.10 T.

The positions of the resistance minima along the $[\bar{1}10]$ and $[110]$ directions can be used to directly extract the magnitude of the CF Fermi wave vectors along $[110]$ and $[\bar{1}10]$ and $[110]$, respectively. According to Eq. (1), $k_F^* = (5/8)(eaB_{\perp}^*/\hbar)$, where B_{\perp}^* indicates the effective CF magnetic field at which the resistance minimum is observed. Note that the commensurability condition along a given modulation direction gives the size of k_F^* in the direction perpendicular to the modulation direction [18,19,34].

Using the above relation, we converted the B_{\perp}^* positions of the resistivity minima seen in Fig. 3 to the size of the CF k_F^* along the $[\bar{1}10]$ and $[110]$ directions and summarize the results in Figs. 4(a) and 4(b). The horizontal, green dashed lines in these figures indicate the expected k_F^* , if a circular CF Fermi contour is assumed. For data taken at $B_{\parallel} = 0$, the values of k_F^* are mostly in good agreement with those expected for CFs with a circular Fermi contour [33]. With increasing B_{\parallel} , however, it is clear in Figs. 4(a) and 4(b) that the CF Fermi wave vector along $[\bar{1}10]$ increases (by as much as 30% at the highest B_{\parallel}), while along $[110]$ it decreases (by nearly 15%). These data therefore provide unambiguous and quantitative evidence for a deformation of the CF Fermi contour in the presence of an applied B_{\parallel} . Moreover, by tilting the sample, the CF anisotropy can be controllably tuned.

We combine the data of Figs. 4(a) and 4(b) to deduce the relative distortion of the CF Fermi contour, as shown in Fig. 4(c). Here, we plot the ratio of k_F^* along the $[\bar{1}10]$ and $[110]$ directions, as deduced from the $B_{\perp}^* > 0$ data. Before performing the division, we fitted each set of data points from Figs. 4(a) and 4(b) with simple, second-order polynomials. The ratio of the two k_F^* values in the two directions is as high as 50% at $B_{\parallel} = 25$ T, indicating a severe distortion as a result of B_{\parallel} . One obvious question that arises is whether the CF Fermi contour is elliptical or has a more complicated (warped) shape, e.g., similar to those we recently measured for 2D holes near zero magnetic field [18]. Since, in our experiments, we measure CF k_F^* only along two specific (and perpendicular) directions, we cannot rule out a complicated shape. However, our data are consistent with a nearly elliptical CF Fermi contour. This is evinced from the plot of Fig. 4(d) where we plot the ratio of the geometric mean of the two k_F^* 's we measure along $[\bar{1}10]$ and $[110]$ to the Fermi wave vector expected for a circular CF Fermi contour, i.e., to $k_F^* = \sqrt{4\pi p}$. The fact that this ratio is close to unity implies that the area enclosed by an elliptical Fermi contour whose major and minor Fermi wave vectors are equal to the two values we measure has the correct magnitude; i.e., it accounts for all the CFs. We show such an ellipse in Fig. 4(c) inset (solid black curve).

The CF commensurability data described here provide the first direct evidence that the CF Fermi contour can be anisotropic. Moreover, they demonstrate how this anisotropy can be tuned via the application of a strong B_{\parallel} . The origin of this anisotropy is very likely the coupling between B_{\parallel} and the out-of-plane motion of the CFs, which have nonzero thickness. Such coupling is known to severely distort the Fermi contour of low-field carriers (Fig. 1). Indeed, for the low-field 2D holes in our samples, we recently measured a very elongated (and nonelliptical) Fermi contour with an anisotropy ratio of about 3 (at $B_{\parallel} = 15$ T), and found the data to be in reasonable agreement with the results of band calculations [18]. The anisotropy

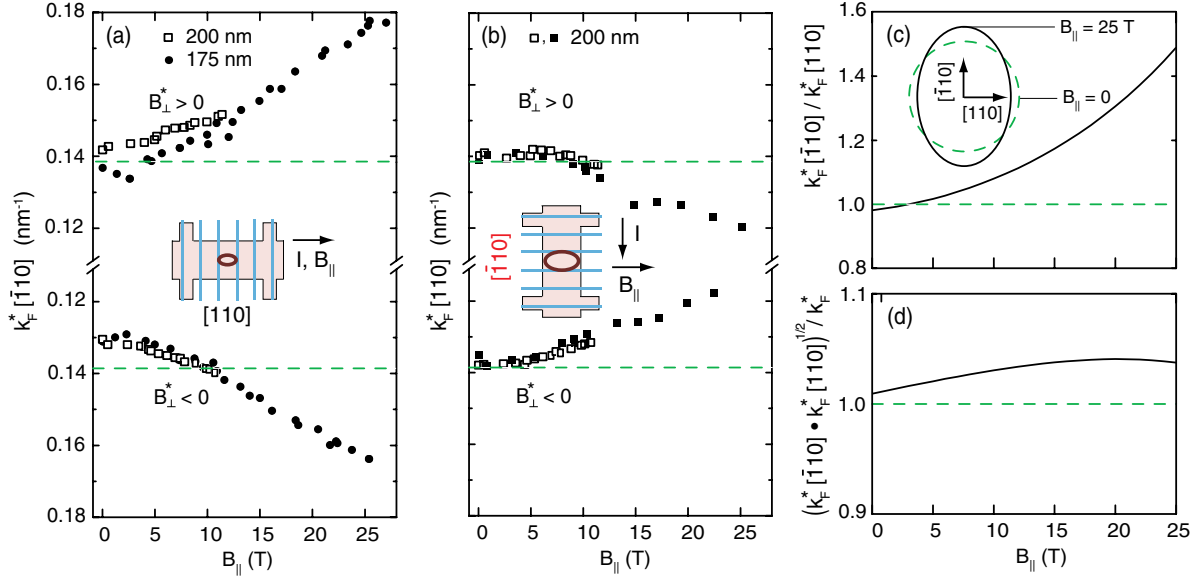


FIG. 4 (color online). (a), (b) Measured values of the CF Fermi wave vectors k_F^* along the $\bar{1}10$ and 110 directions, respectively. Data shown with open squares were measured in a superconducting magnet with a maximum field of 18 T. The closed symbols are data taken in a 31 T resistive magnet system. Horizontal dashed (green) lines represent the Fermi wave vector $k_F^* = \sqrt{4\pi p}$, expected for a circular CF Fermi contour [see Eq. (1)]. The 2D hole density is $p \approx 1.5 \times 10^{11} \text{ cm}^{-2}$. (c) Relative anisotropy of the CF Fermi contour deduced from dividing the (interpolated) measured values of k_F^* along $\bar{1}10$ by those along 110 ; data for $B_{\perp}^* > 0$ were used. The inset schematically shows the CF Fermi contour at $B_{\parallel} = 0$ [dashed (green) circle] and at $B_{\parallel} = 25$ T (solid curve); the latter is based on the assumption that the CF is elliptical. (d) The geometric mean of the measured k_F^* along $\bar{1}10$ and 110 , divided by k_F^* expected for a circular CF Fermi contour.

ratio we measure for the CF Fermi contour at a comparable B_{\parallel} is much smaller, only about 1.2 [Fig. 4(c)]. Absent, however, are theoretical calculations that would treat the anisotropy of CF Fermi contours in the presence of B_{\parallel} in general, and in particular explain the anisotropy we measure in our experiments. The much different anisotropy that we observe for the hole-flux CF Fermi contour compared to the 2D holes indeed appears to contradict the conclusions of the only available theoretical work which predicts that the CF Fermi contour shape should be identical to that of the zero-field particles [11]. We note that, besides its thickness, other parameters of the quasi-2D carrier system, such as the band structure and effective mass as well as the character of the Landau level where the CFs are formed, are also likely to play an important role in determining the anisotropy of the CF Fermi contour in a strong B_{\parallel} . Our conjecture is based on our preliminary data for a 300 Å wide GaAs quantum well containing *electrons*: despite its larger thickness, this sample exhibits a CF Fermi contour anisotropy which is much smaller than the anisotropy we observe in our 175 Å wide GaAs *hole* quantum well sample.

While a quantitative explanation of our experimental data awaits future theoretical work, we emphasize that our results clearly establish the presence of CF Fermi contour anisotropy. This has important implications and raises several interesting questions. For example, what is the role of anisotropic interaction in general? How does the

anisotropy affect the ground states and the excitations of the 2D carrier system at high perpendicular fields? Does the anisotropy affect, e.g., the energy gaps of the fractional quantum Hall states? Our results provide stimulus for future studies to answer some of these questions.

We acknowledge support through the DOE BES (Grant No. DE-FG02-00-ER45841) for measurements, and the Moore and Keck Foundations and the NSF (Grants No. ECCS-1001719, No. DMR-0904117, and No. MRSEC DMR-0819860) for sample fabrication and characterization. This work was performed at the National High Magnetic Field Laboratory, which is supported by NSF Cooperative Agreement No. DMR-0654118, by the State of Florida, and by the DOE. We thank J. K. Jain and R. Winkler for illuminating discussions, and S. Hannahs, T. Murphy, and A. Suslov at NHMFL for valuable help during the measurements. We also thank Tokoyama Corporation for supplying the negative electron-beam resist TEBN-1 used to make the samples.

- [1] *Perspectives in Quantum Hall Effects*, edited by S. Das Sarma and A. Pinczuk (Wiley, New York, 1997).
- [2] M. Shayegan, in *High Magnetic Fields: Science and Technology*, edited by F. Herlach and N. Miura (World Scientific, Singapore, 2006), Vol. 3, pp. 31-60.
- [3] J. K. Jain, *Composite Fermions* (Cambridge University Press, Cambridge, England, 2007).

- [4] J. K. Jain, *Phys. Rev. Lett.* **63**, 199 (1989).
- [5] B. I. Halperin, P. A. Lee, and N. Read, *Phys. Rev. B* **47**, 7312 (1993).
- [6] R. L. Willett, R. R. Ruel, K. W. West, and L. N. Pfeiffer, *Phys. Rev. Lett.* **71**, 3846 (1993).
- [7] W. Kang, H. L. Stormer, L. N. Pfeiffer, K. W. Baldwin, and K. W. West, *Phys. Rev. Lett.* **71**, 3850 (1993).
- [8] V. J. Goldman, B. Su, and J. K. Jain, *Phys. Rev. Lett.* **72**, 2065 (1994).
- [9] J. H. Smet, D. Weiss, R. H. Blick, G. Lutjering, K. von Klitzing, R. Fleischmann, R. Ketzmerick, T. Geisel, and G. Weimann, *Phys. Rev. Lett.* **77**, 2272 (1996).
- [10] Throughout this Letter, we use * to denote the CF parameters.
- [11] D. B. Balagurov and Yu. E. Lozovik, *Phys. Rev. B* **62**, 1481 (2000).
- [12] T. Gokmen, M. Padmanabhan, and M. Shayegan, *Nat. Phys.* **6**, 621 (2010).
- [13] J. Xia, J. P. Eisenstein, L. N. Pfeiffer, and K. W. West, *Nat. Phys.* **7**, 845 (2011).
- [14] M. Mulligan, C. Nayak, and S. Kachru, *Phys. Rev. B* **82**, 085102 (2010); **84**, 195124 (2011).
- [15] B. Yang, Z. Papic, E. H. Rezayi, R. N. Bhatt, and F. D. M. Haldane, *Phys. Rev. B* **85**, 165318 (2012).
- [16] R. Z. Qiu, F. D. M. Haldane, X. Wan, K. Yang, and S. Yi, *Phys. Rev. B* **85**, 115308 (2012).
- [17] H. Wang, R. Narayanan, X. Wan, and F. Zhang, *Phys. Rev. B* **86**, 035122 (2012).
- [18] D. Kamburov, M. Shayegan, R. Winkler, L. N. Pfeiffer, K. W. West, and K. W. Baldwin, *Phys. Rev. B* **86**, 241302 (R) (2012).
- [19] D. Kamburov, H. Shapourian, M. Shayegan, L. N. Pfeiffer, K. W. West, K. W. Baldwin, and R. Winkler, *Phys. Rev. B* **85**, 121305(R) (2012).
- [20] E. Skuras, A. R. Long, I. A. Larkin, J. H. Davies, and M. C. Holland, *Appl. Phys. Lett.* **70**, 871 (1997).
- [21] A. Endo, S. Katsumoto, and Y. Iye, *Phys. Rev. B* **62**, 16761 (2000).
- [22] A. Endo, M. Kawamura, S. Katsumoto, and Y. Iye, *Phys. Rev. B* **63**, 113310 (2001).
- [23] A. Endo and Y. Iye, *Phys. Rev. B* **72**, 235303 (2005).
- [24] D. Kamburov, M. Shayegan, L. N. Pfeiffer, K. W. West, and K. W. Baldwin, *Phys. Rev. Lett.* **109**, 236401 (2012).
- [25] R. L. Willett, K. W. West, and L. N. Pfeiffer, *Phys. Rev. Lett.* **83**, 2624 (1999).
- [26] J. H. Smet, D. Weiss, K. von Klitzing, P. T. Coleridge, Z. W. Wasilewski, R. Bergmann, H. Schweizer, and A. Scherer, *Phys. Rev. B* **56**, 3598 (1997).
- [27] J. H. Smet, K. von Klitzing, D. Weiss, and W. Wegscheider, *Phys. Rev. Lett.* **80**, 4538 (1998).
- [28] A. D. Mirlin, P. Wolfle, Y. Levinson, and O. Entin-Wohlman, *Phys. Rev. Lett.* **81**, 1070 (1998).
- [29] F. von Oppen, A. Stern, and B. I. Halperin, *Phys. Rev. Lett.* **80**, 4494 (1998).
- [30] J. H. Smet, S. Jobst, K. von Klitzing, D. Weiss, W. Wegscheider, and V. Umansky, *Phys. Rev. Lett.* **83**, 2620 (1999).
- [31] S. D. M. Zwerschke and R. R. Gerhardts, *Phys. Rev. Lett.* **83**, 2616 (1999).
- [32] More generally, the commensurability condition is $2R_C^*/a = i + 1/4$ where $i = 1, 2, 3, \dots$; i.e., minima in magnetoresistance are expected whenever the cyclotron diameter $2R_C^*$ becomes commensurate with an integer multiple of the period a . Throughout our Letter, we focus on the primary resistance minimum ($i = 1$), although in some of our data we do observe a weak resistance minimum corresponding to $i = 2$ (see, e.g., the resistance minimum at $|B_\perp^*| \approx 0.5$ T in the data of Fig. 3(a); also, see Ref. [24]).
- [33] For $B_\perp^* > 0$, the expected positions of the resistance minima at $B_\parallel = 0$ match the observed positions well while for $B_\perp^* < 0$ the observed minima are sometimes slightly shifted toward $B_\perp^* = 0$ [see, e.g., the lower trace in Fig. 3(a)]. We have seen similar shifts in several of our 2D hole samples [see, e.g., Fig. 2(a) of Ref. [24]]; a similar shift was also observed in electron samples and was attributed to the mixing of the electrostatic and magnetic commensurability conditions [27].
- [34] O. Gunawan, Y. P. Shkolnikov, E. P. De Poortere, E. Tutuc, and M. Shayegan, *Phys. Rev. Lett.* **93**, 246603 (2004).